Chinese Chemical Letters 32 (2021) 3940–3947

Contents lists available at ScienceDirect

Chinese Chemical Letters

journal homepage: www.elsevier.com/locate/cclet

Communication

A porous hydrogel scaffold mimicking the extracellular matrix with swim bladder derived collagen for renal tissue regeneration

Heng Wu[a,b], Rui Zhang[a,b], Bianxiang Hu[a], Yutong He[b], Yuehang Zhang[a,b], Liu Cai[c], Leyu Wang[c], Guobao Wang[a,*], Honghao Hou[b,*], Xiaozhong Qiu[b,*]

[a] State Key Lab for Organ Failure Research, National Clinical Research Center of Kidney Disease, Division of Nephrology, Nanfang Hospital, Southern Medical University, Guangzhou 510515, China
[b] Guangdong Provincial Key Laboratory of Construction and Detection in Tissue Engineering, School of Basic Medical Sciences, Southern Medical University, Guangzhou 510515, China
[c] Biomaterials Research Center, School of Biomedical Engineering, Southern Medical University, Guangzhou 510515, China

ARTICLE INFO

Article history:
Received 20 February 2021
Revised 20 April 2021
Accepted 22 April 2021
Available online 28 April 2021

Keywords:
Swim bladder
Collagen I
Chondroitin sulfate
Extracellular matrix-mimicking hydrogel
Renal tissue regeneration

ABSTRACT

As a worldwide public health issue, chronic kidney disease still lacks of effective therapeutic approaches due to the challenges in conventional organ transplantation and dialysis. Renal tissue engineering offers an advantageous therapeutic or regenerative option over typical donor organ. However, despite the great progress of decellularized extracellular matrix based scaffold for the renal regeneration, several safety concerns and complex composition still remain to be addressed. Herein, the extracellular matrix-mimicking hydrogel scaffolds were developed through covalent and physical cross-linking between swim bladder-derived natural collagen (COL) and anti-fibrosis chondroitin sulfate (CS) derivatives. The biomimetic hydrogels showed proper mechanical property, excellent thermal stability and high biocompatibility both *in vitro* and *in vivo*, by altering the mass ratio of COL and CS. When implanted in partially nephrectomized rat model, the 1COL/2CS scaffold enable it recruit more native kidney cells, reduce the tubular damage, and even induce the regeneration of renal tubular-like tissue and restore renal metabolic function more effectively comparing with the pure 2COL and 2CS scaffold. These results suggest that the biomimetic scaffold is a promising functional platform for treating renal diseases.

© 2021 Published by Elsevier B.V. on behalf of Chinese Chemical Society and Institute of Materia Medica, Chinese Academy of Medical Sciences.

The chronic kidney disease (CKD), defined by declined renal function and/or damaged renal structure [1], is growingly identified as a public health issue due to the high incidence and prevalence globally, affecting approximate 8%–16% of people worldwide [2]. Despite the constantly rising incidence, the available treatment for CKD is still limited. Dialysis has the capability to partially substitute renal filtration function through clearing certain metabolic wastes from the blood, but dialysis frequently gives rise to an inferior life's quality for a long-term surviving patient and is poorly tolerated [3]. When CKD develops into end-stage renal disease (ESRD), kidney transplantation is the only effective therapeutic approach, but the shortage of donated organs and the adverse effects in long-term usage of immunosuppressants restrict its extensive clinical practice [4]. To address these problems, *in situ* regeneration strategy through offering an inductive template to guide cellular behaviors, recellularization and functional organ recovery in the injured area may be a promising renal therapeutic approach.

Decellularized extracellular matrix (dECM) had been proved as a promising scaffold in aspect of renal regeneration [5]. However, the indisciplinable residual cell debris and other immunogenic substances in dECM scaffold always lead to dECM-invoked host reactivity under the condition of inadequate and nonstandard protocol of decellularized tissue. The dECM-invoked host reactivity and implanted-scaffold rejection remain to be investigated [6]. Hydrogel is an appealing candidate for mimicking ECM as a promising 3D porous network scaffold for cell adhesion [7] and is widely applied in the biomedical fields due to its prominent characteristics such as controllable physical and chemical properties, biology-relative physical signals delivery and high biocompatibility [8–10]. Both collagen I (COL I) and chondroitin sulfate (CS) are key structural compositions in the kidney ECM [11–13]. Especially, CS is involved in the synthesis of proteoglycan, which acts a vital role in diverse biological phenomena like cell migration [14] and growth factor binding [15]. Hence, we designed a CS-based biomimetic

* Corresponding authors.
E-mail addresses: nfyywanggb@163.com (G. Wang), ss.hhh89@hotmail.com (H. Hou), qqiuxzh@163.com (X. Qiu).

https://doi.org/10.1016/j.cclet.2021.04.043
1001-8417/© 2021 Published by Elsevier B.V. on behalf of Chinese Chemical Society and Institute of Materia Medica, Chinese Academy of Medical Sciences.

porous hydrogel scaffold incorporated with COL I as a template to effectively induce renal regeneration.

The diverse inherent properties of COL I endow it with the capacity to form 3D-like network scaffolds and enable it as a natural option in fields of tissue engineering scaffolds [13]. The main common sources of COL I comprise porcine skin, bovine skin, bone and tendons, and rat tail [16]. However, religious beliefs in certain regions and concerns about the transmissible diseases such as bovine spongiform encephalopathy, swine flu and other zoonose diseases restrict the use of land animal collagens [17]. Recently, as an alternative source, fish collagen has obtained increasing attention, for recycling of abundant fish offal, avoiding zoonose diseases, debarring religious objections and especially its low immunogenicity [18]. Herein, we chose swim bladder collagen from the grass carp to develop a biomimetic hydrogel. A previous study had demonstrated that mesangial cells (MCs) seeded on COL I derived gels gave rise to increased expression of COL I, fibronectin (Fn) and transforming growth factor beta 1 (TGF-β1), suggesting that pure COL I derived hydrogel could alter cell behaviors and functions [19]. CS is a representative class of glycosaminoglycan (GAG) [20], which extensively distributes in various organism extracellular matrices and participates in formation of proteoglycans by covalent links with proteins [21]. The invertebrate GAG could reduce the recruitment of inflammatory cells and attenuate interstitial fibrosis [22]. CS has attracted lots of attention in the application of tissue engineering because of its favorable biocompatibility, anti-fibrotic [23,24] and anti-inflammatory [25] effects. In consideration of the fibrogenic feature of COL I, we fabricated the biomimetic porous hydrogels based on CS incorporating with COL I derived from the swim bladders in grass carp. The fabricated hydrogels were then implanted into the partially nephrectomized areas of the rats and evaluated by histological stains and renal metabolic molecular levels.

Type I collagen was extracted from the swim bladder of grass carp according to the previously reported protocol [26]. Briefly, the fresh swim bladders were washed several times with distilled water to remove the muscle and vascular tissue attached on the surface. For removal of non-collagenous proteins, the swim bladders were rinsed in 2.5% sodium chloride solution and then 0.1 mol/L sodium hydroxide solution under stirring for 6 h, respectively. Next, the swim bladders were rinsed several times with deionized water until approximate pH 7 and further soaked into 0.5 mol/L acetic acid solution for 12 h under stirring for collagen extraction. The acetic acid solution containing extracted collagen was dialyzed against deionized water for 3–4 days until gelation physically. The gelation was freeze-dried and stored at −20 °C until further use.

To analyze the structural information of extracted collagen from natural swim bladder, dodecyl sulfate-polyacrylamide gel electrophoresis (SDS-PAGE) was performed by the following procedures. Lyophilized collagen was dissolved in distilled water (10 mg/mL) at 50 °C under stirring. For protein denaturation, the solutions were mixed in 4:1 (v/v) with loading buffer and then heated 7 min at 100 °C. After complete denaturation, 12 μL of the mixture and 3 μL of protein marker were loaded onto SDS-PAGE gel, respectively. Both 8% separating gel and 5% stacking gel were run for 0.5 h at 80 V and 1 h at 120 V. After running, the gel was stained in a 0.25% Coomassie staining solution (0.25 g Coomassie Brilliant Blue R-250, 45 mL absolute ethyl alcohol, 10 mL glacial acetic acid and 45 mL deionized water) for 1 h. Excess stain was removed with destainer (50 mL absolute ethyl alcohol, 100 mL glacial acetic acid and 850 mL deionized water) for 6 h under stirring, and the destainer was changed each hour. The gel with the bands was photographed for further analysis.

Methacrylamide functionalized collagen (COL-MA) was prepared by reaction of freeze-dried COL I with methacrylic anhydride (MA). 2 g of lyophilized COL I was dissolved in 40 mL of phosphate buffer solution (PBS, pH 7.5) at 50 °C, 4 mL of methacrylic anhydride was added dropwise to the solution under vigorously stirring. After 2 h of reaction, the reaction mixture was diluted with three-folds PBS and dialyzed for 3–4 days against deionized water. The dialyzed product was freeze-dried and then stored at −20 °C until further use.

Chondroitin sulfate-methacrylate (CS-MA) was synthesized by CS (Solarbio) and methacrylic anhydride. In detail, 5 g of CS powder was dissolved completely in the 100 mL distilled water, and then 10 mL of methacrylic anhydride was added dropwise under vigorously stirring. The pH value of the reaction mixture was controlled at 8.0 by adding 5 mol/L NaOH solution. After being stirred at 4 °C for 24 h, the reaction mixture was dialyzed against deionized water for 4 days. The dialyzed product was freeze-dried and stored at −20 °C until further use.

2% w/v COL-MA, 1% w/v COL-MA/2% w/v CS-MA, 0.5% w/v COL-MA/2% w/v CS-MA and 2% w/v CS-MA were respectively dissolved in distilled water under stirring at room temperature (named as 2COL, 1COL/2CS, 0.5COL/2CS, 2CS, respectively). 2 μL of 10% w/v ammonium persulphate solutions (APS) and 1 μL of *N,N,N',N'*-tetramethylethylenediamine (TEMED) were added in sequence as polymerization initiator and accelerant to the 100 μL of above pre-solutions in cylindrical molds. After blending the reactive mixture adequately, put the cylindrical molds into −20 °C freezer overnight to form 2-mm-height and 1-cm-diameter disk hydrogels. Then, the hydrogels were immersed into deionized water to remove residual unreactive cross-linking agent for 2 days and the water was changed each 4 h.

The chemical compositions of products that COL or CS reacted with methacrylic anhydride were verified by the Fourier transform infrared (FTIR) spectroscopy (Nicolet iS50, USA). The spectra were analyzed in the ranges from 4000 cm^{-1} to 500 cm^{-1}.

The porous structure of hydrogels was characterized by scanning electron microscope (SEM, ZEISS ULTRA 55, Japan). The pore diameters of hydrogels were calculated by the Image J software.

The thermal stability in the hydrogel was measured *via* TGA (NETZSCH TG 209F1 Libra, Germany). The hydrogels were kept dry under vacuum prior to analysis. Under continuous nitrogen atmosphere, the precisely weighed sample was heated from 30 °C to 800 °C at heating rate of 10 °C/min and the remanent weight was obtained.

After being weighed, the lyophilized hydrogels were immersed in distilled water at room temperature until swelling equilibrium. The swollen hydrogels were weighed and recorded at fixed time points after absorbing excess water on the surface with a filter paper. The swelling ratio at each time intervals was calculated by $(W_s-W_d)/W_d$ (4 samples/group were tested), where W_d was the weight of the freeze-dried hydrogel and W_s was the weight of the swollen hydrogel.

The mechanical behaviors of the hydrogels were tested using a universal testing machine (AMETEK LS1, USA) at 2 mm/min rate. All operations were performed at room temperature. The stress–strain curves of hydrogels were obtained through analyzer software. The elastic modulus was calculated from the initial 10 to 20% of the linear region of the stress–strain curves. At least 6 samples in each group were tested and the data was analyzed through GraphPad Prism 8 and Origin 8 software.

Rat renal mesangial cells (RMCs) and human kidney proximal tubular epithelial cells (HK-2) were purchased from the cell bank of Chinese Academy of Sciences (Shanghai). The hydrogels were sterilized at high temperature and pressure by autoclave. 80 μL of cell suspension with a concentration of 1×10^6 cells/mL were seeded onto sterile hydrogel dropwise and then incubated for 2 h for cells attachment to the hydrogel. Cells were cultured with low-glucose DMEM (obtained from Gibco) supplemented with 10% fetal bovine serum (FBS, Gibco), 100 U/mL penicillin and 100 μg/mL

streptomycin at 37 °C in a 5% CO_2 incubator. The medium was changed every 2 days.

The biocompatibility of the hydrogel was examined *via* live/dead staining. At the determined time point (day 1, day 3, day 5), the hydrogels containing RMCs or HK-2 cells were rinsed three times with PBS and then stained with the live/dead working solution (provided by Life technologies) for 10 min at room temperature in the dark. The dyed samples were imaged with a laser scanning confocal microscope (Leica, Germany). The calcein-AM green fluorescence stained live cells and the ethidiumhomodimer-1 red fluorescence marked dead cells.

RMCs were seeded on the hydrogels for 3 days and then fixed in 2.5% glutaraldehyde at 4 °C overnight. The samples were rinsed three times in PBS (10 min each time), subsequently dehydrated in gradient series of ethanol (50%, once for 10 min; 70%, overnight; 90%, once for 10 min; 100%, three times, each for 10 min.) and dried in a way of supercritical drying. Finally, the samples were sputtered with gold, then imaged and photographed by SEM.

After being cultured for 3 days, the hydrogels seeded RMCs were fixed with 4% paraformaldehyde (obtained from Leagene) overnight at 4 °C. Following being washed three times in PBS, the samples were permeated with 0.2% Triton X-100 at room temperature for 10 min, and then blocked with 2% bovine serum albumin (BSA) at room temperature for 1 h. Subsequently, the samples were incubated with mouse anti-α-SMA (1:200, abcam) and rabbit anti-Fn (1:200, abcam) at 4 °C overnight. After being rinsed three times in PBS, the samples were incubated with Alexa Fluor 488 donkey anti-mouse IgG (H&L, 1:500) and Alexa Fluor 568 donkey anti-rabbit IgG (H&L, 1:500, Molecular Probes) for 2 h at room temperature, then washed with PBS, sequentially stained with 4′, 6-diamidino-2-phenylindole (DAPI, Leagene) for 1 h and finally imaged with laser scanning confocal microscope. For F-actin staining, after being permeated, the cells were stained with 500 nmol/L fluorescein isothiocyanate phalloidin (AAT Bioquest) for 30 min and then DAPI followed by rinsing with PBS. The samples were examined for three independent biological experiments. The intensity of immunoreactivity was calculated by ImageJ software.

After being cultured for 3 days, the hydrogels seeded RMCs were washed three times with PBS and then ground in liquid nitrogen. The proteins were extracted using total protein extraction kit. The proteins (20−50 μg per lane) were electrophoresed on 10% separating gel and then transferred onto PVDF membranes electrophoretically. The membranes were blocked with 5% skim milk (w/v) in TBS-T buffer for 2 h at room temperature and then incubated with primary antibody against Fn (1:5000) at 4 °C overnight, subsequently, rinsed three times with TBS-T buffer (10 min each time) and finally incubated with the corresponding peroxidase-conjugated secondary antibody (1:5000) for 2 h at room temperature. The protein bands were detected by Super ECL Detection Reagent (Shang Hai Yeasen Biological Technology, China) according to the manufacturer's instructions. GAPDH was used as an internal reference. The samples were examined for three independent biological experiments and the gray values were analyzed by ImageJ software.

All the animal experiments were approved by Animal Ethics Committee in Southern Medical University under the Regulations for the Administration of Affairs Concerning Experimental Animals (PR China). Male Sprague Dawley rats (weight: 160-200 g) were divided into five groups randomly: the sham group, the injury group (partially nephrectomized but not implanted with any scaffold) and the groups implanted with scaffolds including 2COL group, 1COL/2CS group and 2CS group. Every rat was anesthetized *via* intraperitoneal injection of chloral hydrate (0.3 g per kilogram body weight). Expose the renal from the back incision and then rip the renal capsule gently through a surgical operation. After ligation of the right renal pedicle, the right renal was completely removed. The left renal artery and vein were clipped with microligation haemostatic clip, at which point the timer began to assure that renal ischemia was kept within 10 min. The left kidney was transected slightly above the renal pelvis (removing about 1/3 of the renal parenchyma), and then the scaffold was immediately implanted into the defected site of the left renal. After reperfusion and hemorrhage stopping in renal, the abdominal wall was closed. The operated rats were collected blood from the heart at 4 and 8 weeks for renal function analysis and sacrificed at 8 weeks after the operation, and the scaffold and its surrounding tissue were extracted for further histology analysis.

After 8 weeks of operation, histological analysis was performed including the degree of fibrosis, inflammation-related cell infiltration and regenerated kidney tissue morphology assessment. 2 μm of paraffin-embedded kidney sections were subjected to Masson and H&E staining using commercial kits (Sigma-Aldrich, USA) according to the manufacturer's protocol. To evaluate renal function, blood urea nitrogen (BUN) and serum creatinine levels were examined (at 4, 8 weeks) by the fully automatic biochemical analyzer (Beckman Coulter AU480, USA). All the stained tissue sections were imaged by the pathological slide scanner (Leica, USA).

All tests were operated at least three times. The data were showed as mean ± standard deviations. Statistical analysis was performed using Student's test by GraphPad Prism 8 software. Differences were considered to be significant at $P < 0.05$.

After successfully extracting collagen protein from the swim bladder, we used sodium dodecyl sulfate-polyacrylamide gel electrophoresis (SDS-PAGE) to analyze structural information and purity of the obtained protein sample (Fig. 1a). Electrophoresis analysis displayed the characteristic bands of collagen I that were one β chain (the dimer) at 250 kDa and two different α chains (α1 and α2) at approximate 130 kDa, and α1 chain was two times more intense than α2 chain.

Then, the chondroitin sulfate-methacrylate (CS-MA) and collagen-methacrylamide (COL-MA) were synthesized by the reactions of CS and lyophilized COL I with methacrylic anhydride, respectively. The chemical structures of obtained COL-MA and CS-MA were characterized by FTIR spectra. As shown in Fig. 1b, the characteristic absorption peak for functionalized COL-MA including the stretching vibration of −C=O bond, bending vibration of N–H bond and plane vibration of C–N and N–H bond appeared at corresponding 1652.45 cm^{-1} (amide I), 1543.59 cm^{-1} (amide II) and 1455 cm^{-1} (amide III). Compared with that of pure COL I group (1653 cm^{-1}), the characteristic peak at 1652 cm^{-1} corresponding to the amide I has a little shift, and the intensity of absorption peaks at C–H stretching and bending area and the amide I demonstrated an obvious increase in the FTIR spectrum of COL-MA, which is consistent with other reported references [10], confirming that the successful binding of MA to the amine groups of COL. From Fig. 1c, we can see that a new characteristic peak appeared at 1718.37 cm^{-1}, which should be assigned to –O–C=O (ester bond) stretching, which was absent in the spectrum of CS, indicating the successful synthesis of CS-MA. Finally, four kinds of hydrogels, including 2COL (2% w/v COL-MA), 1COL/2CS (1% w/v COL-MA and 2% w/v CS-MA), 0.5COL/2CS (0.5% w/v COL-MA and 2% w/v CS-MA), 2CS (2% w/v CS-MA), were prepared in cylindrical molds *via* chemical crosslinking between collagen-methacrylamide (COL-MA) and chondroitin sulfate-methacrylate (CS-MA), respectively.

Next, the four groups of hydrogels were characterized in terms of pore structure, thermal stability, swelling and mechanical properties, as these characteristics are crucial for hydrogel scaffolds used for *in vitro* culture or *in vivo* implantation.

To better understand the porous microstructures of biomimetic hydrogels with different CS/COL contents, we examined the corresponding surface microstructures of as-prepared hydrogels by

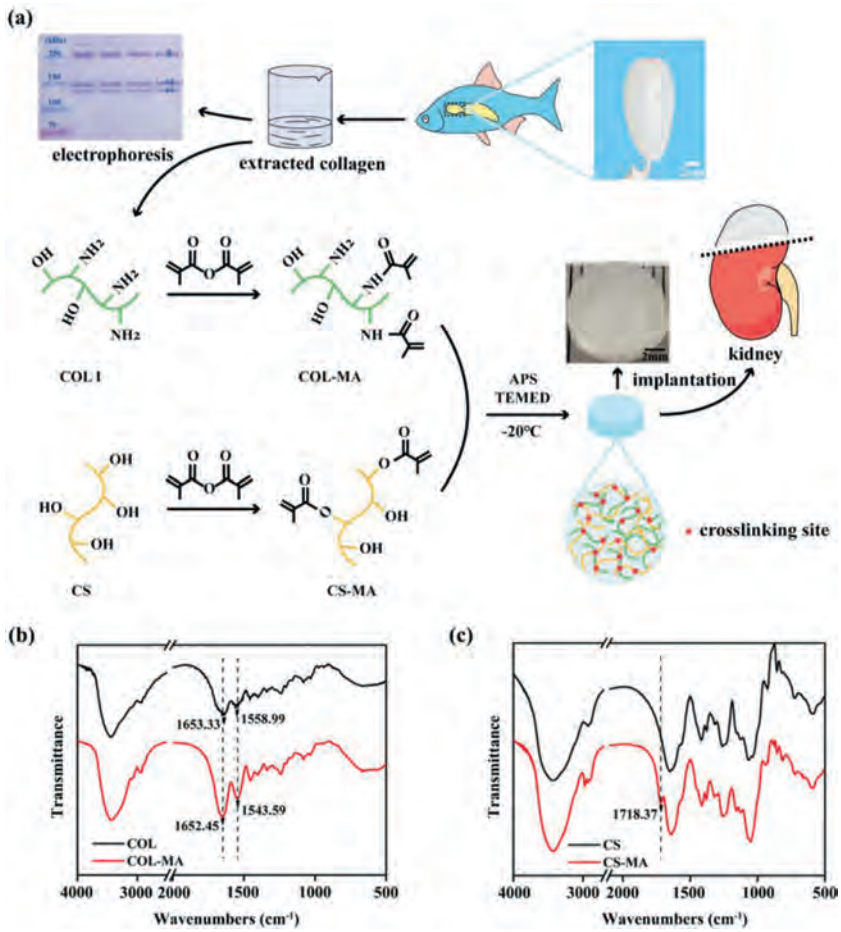

Fig. 1. (a) Schematic illustration of constructing the biomimetic hydrogel scaffold for renal tissue regeneration and involved chemical structures and reactions. (b, c) Verifying the chemical structural information of different target compounds COL-MA (b) and CS-MA (c) with pure COL and CS as reference revealed by Fourier transform infrared spectroscopy (FTIR), respectively.

SEM. As presented in Fig. 2a, the lyophilized 2COL, 1COL/2CS, 0.5COL/2CS and 2CS hydrogel exhibited open-porous structure with a similarly high porosity and abundant interconnected or secondary pores, which is critical for ensuring sufficient 3D space for cell proliferation and growth as tissue engineering scaffolds. In comparison, with a relatively homogeneous pore sizes of about 100 μm, the groups 2COL and 1COL/2CS were equipped with larger pore sizes in comparison with the other two groups, and the mean pore diameter in 1COL/2CS was bigger slightly than 2COL group (Fig. 2b). Except the bioactive macromolecules cross-linking with each other, placing reactive solutions immediately in a refrigerator at −20 °C to gel after mixing contribute greatly to homogeneous pore conformation [27]. The pore size, volume and porosity are important elements to fabricate an ideally 3D porous hydrogel scaffold in the field of tissue engineering [28]. In addition, the large pore and high porosity of the hydrogel can facilitate diffusion of nutrients and removal of metabolic waste products [29] as well as expose the more cells to a 3D-like surrounding with the average pore size of approximately 100 μm [30]. Nevertheless, many reports are not unanimous, as diverse cells are seeded on the different kinds of porous scaffolds applied to various aspects in tissue engineering [31].

The thermally stability and degradation properties of the hydrogel scaffolds was further analyzed *via* thermogravimetric analysis (TGA). As hydrogels were vastly studied in biomedical application, the thermal stability of biomaterial was considered increasingly as an indispensable environmental factor because of constant supply of heat energy to the hydrogels in order to keep homoeothermic at approximately 37 °C for *in vivo* scaffold transplantation or *in vitro* cell culture [32]. The thermogravimetric curves of 2COL, 2CS and COL/CS mixed scaffolds were presented in Fig. 2c. With the temperature going up, consistently, the four group hydrogels exhibited a sharp drop in the temperature ranges from 200 °C to 400 °C. The results exhibited a similar thermal stability as there was no significant difference between the four kind of hydrogel scaffolds in initial decomposition temperature and melting temperature.

The swelling characteristics of the hydrogels were checked by typical swelling experiment as shown in Fig. 2d. Generally, there were little changes in the swelling volume of the four group hydrogels, so after being implanted into the rats' bodies, the volume of the hydrogels did not get too big because of the exudation. The hydrogels containing the composition-CS reached swelling equilibrium rapidly within a few minutes in distilled water at room temperature. Additionally, among the groups 1COL/2CS, 0.5COL/2CS and 2CS, the swelling mass ratios before and after swelling were higher than that of the 2COL hydrogel group and the ratio got increased with decreasing mount of COL I, demonstrating that CS was endowed with better hydrophilicity. The ability of the hydrogel to draw and retain water is dependent on many factors like the hydrophilicity of the material, porosity of the scaffold and chemical cross-linking intensity [33]. The swelling characteristic of the hydrogel network is also crucial in a variety of biomedical engineering applications as it affects solute diffusion, mechanical properties and the overall shape of patterned hydrogels [34].

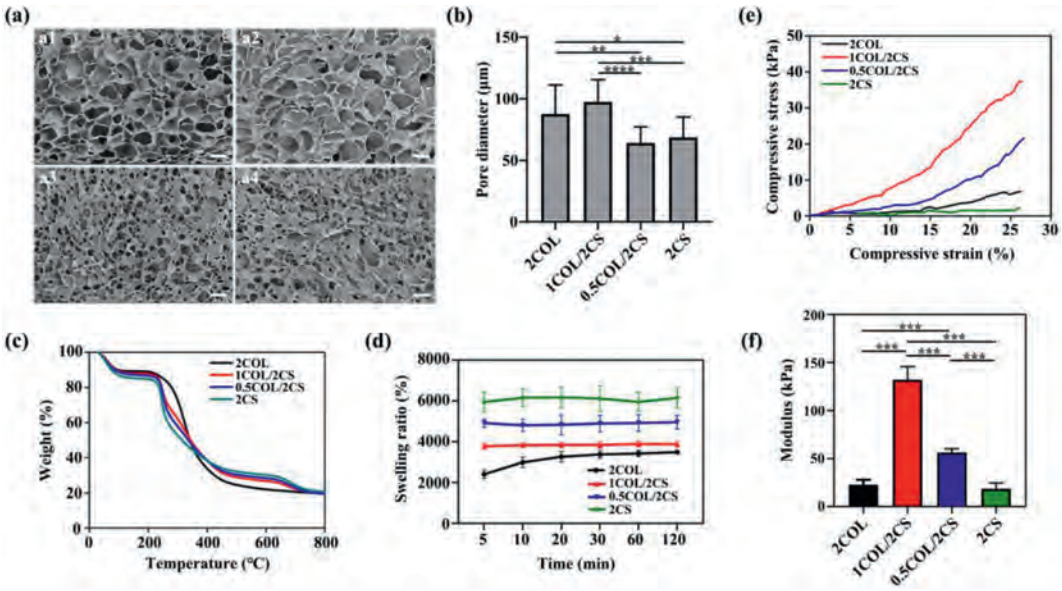

Fig. 2. Characterizations of different hydrogel scaffolds consisting of COL and/or CS. (a, b) SEM images (scale bars, 100 μm) and the statistical analysis of pore diameter of 2COL (a1), 1COL/2CS (a2), 0.5COL/2CS (a3) and 2CS (a4) hydrogel. (c) TGA thermograms and (d) swelling ratio at room temperature. (e) Compressive stress-strain curves and (f) modulus of diverse biomimetic hydrogels. Values are illustrated as mean ± SD. $^{*}P < 0.05$, $^{**}P < 0.005$, $^{***}P < 0.0005$, $^{****}P < 0.0001$.

Moreover, considering the requirements of biological tissue, appropriate mechanical properties of scaffold materials, are crucial for the adhesion, proliferation, migration and differentiation of seed cells [35]. The mechanical properties of the 2COL, 2CS, 0.5COL/2CS, and 1COL/2CS hydrogels were characterized using compression test and compressive modulus method during compression to 20% strain. Figs. 2e and f displayed the compressive stress-strain curves of the four group hydrogels and corresponding Young's modulus (strain 10%–20%). As shown in Fig. 2e, the four hydrogels of 2COL, 2CS, 0.5COL/2CS, and 1COL/2CS group exhibited quite soft and flexibility with the compressive strain of less than 30%. The graph in Fig. 2f showed that the 2COL, 2CS, 0.5COL/2CS, and 1COL/2CS hydrogel had a compressive modulus of 22.6 ± 0.049, 18.6 ± 0.055, 56.5 ± 0.033, and 132.2 ± 0.123 kPa at the 10%−20% strain region, respectively. Overall, all the Young's modulus values of the hydrogels were smaller than that of reported scaffolds in renal tissue engineering, which may be more proper for soft renal tissue [31]. The pure 2CS hydrogel is fragile with the compressive modulus of only 18.6 kPa, while the pure 2COL hydrogel is much tougher than the pure 2CS hydrogel, with the compressive modulus of 22.6 kPa. By comparison, the 1COL/2CS (~132 kPa) and 0.5COL/2CS hydrogels (~56 kPa) are greatly strengthened by forming a semi-interpenetrating polymer network (semi-IPN) or interpenetrating polymer network (IPN) structure due to more noncovalent interaction such as hydrogen and ion bonding between COL and CS. 1COL/2CS hydrogel shows the highest Young's modulus with the value of ~132 kPa, ~7 times higher than that of pure 2COL and 1COL/2CS hydrogel, showing a relatively high toughness and better potential for bio-scaffolds. 1COL/2CS hydrogel exhibits higher compressive modulus, which might be ascribed to its increased crosslinking density and consequently the higher water uptake content. These results showed that the bionic 1COL/2CS hydrogels can be regarded as the promising alternative materials as a result of their proper mechanical properties for soft renal tissue and having a 3D elastic network with hydrophilic characteristic that simulate native ECM structure [36]. Mechanical properties of the matrix environment have been shown to affect cell function and behavior including cell proliferation, migration and differentiation [35]. For instances, a research demonstrated that mechanical properties had a great influence on podocytes' differentiation and phenotype state such as nephrin and podocin expression which was closely related to their filtration function [37]. Mesenchymal stem cells were extremely susceptible to tissue structure elasticity in phenotypes and had capacity to differentiate into specify lineage relying to certain elastic modulus, as MSCs differentiated into cells with neurogenic phenotype when seeded on the soft biomaterials and expressed osteogenic phenotype once cultured on relatively stiff matrices [38]. Our proposed hydrogel scaffolds' compressive modulus from 2CS, 2COL to mixed group (0.5COL/2CS, 1COL/2CS) corresponding to ~18, ~22, ~56, ~132 kPa exhibited soft-mechanical property which is beneficial for renal tissue regeneration.

As biocompatibility is a fundamental requirement for tissue engineering, live/dead staining assays were performed to evaluate the cytocompatibility on the hydrogel scaffolds. Cell viabilities of RMCs (Fig. 3a) and HK-2 cells (Fig. S1 in Supporting information) on different hydrogels were illustrated and cell morphology was measured by F-actin staining (Fig. 3b) and SEM (Fig. S2 in Supporting information). As results, more than 95% cells survived in each hydrogel on day 1, day 3, day 5, respectively. The four group hydrogels themselves were nontoxic and biocompatible. However, compared with those in 2COL, 1COL/2CS and 0.5COL/2CS groups, great quantities of round cells and less numbers of stretched cells located into the hydrogel in 2CS group. With the increase of COL I in hydrogel, the located cells grew faster and tended to be more stretched. As reported, CS could inhibit cell adhesion [39], and this property has been applied for the prevention of post-operation adhesion [40]. Therefore, the 2CS hydrogel comprising pure CS was not appropriate for cell migration and adhesion.

The high porosity, appropriate mechanical properties and good cytocompatibility inspired the further study for functional repair potential of the hydrogel scaffolds after renal injury. Anti-fibrosis property of scaffolds materials is beneficial for functional renal repair. Therefore, the expression of fibrosis-related proteins from different hydrogels was examined by immunofluorescence (Fig. 4) and western blot (Fig. 5a) analysis. As presented in Fig. 4, the fluorescence intensity of both Fn and α-SMA in 2COL group was almost three times higher than that in the other three groups, while no obvious difference was detected among 1COL/2CS, 0.5COL/2CS and 2CS groups. Similar to immunofluorescence analysis, higher

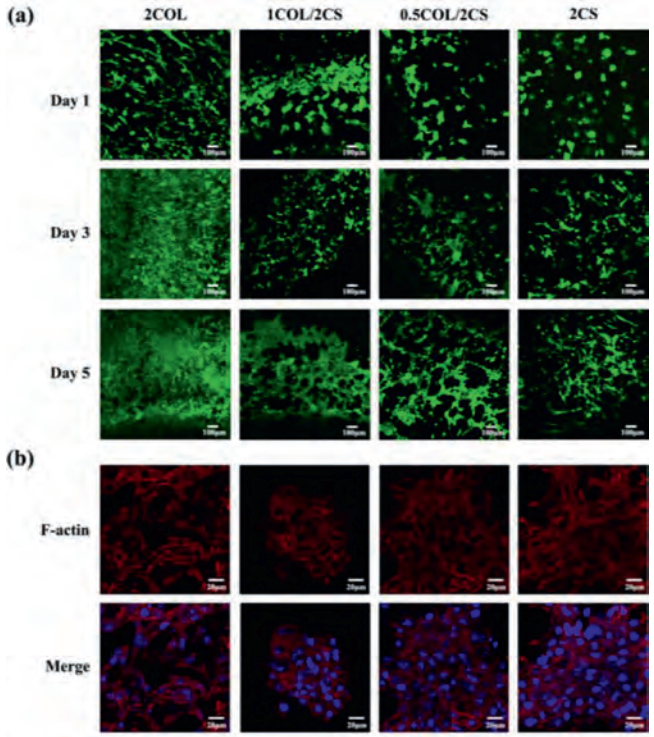

Fig. 3. Biocompatibility and cell morphology in various hydrogel scaffolds. (a) Live/dead staining of RMCs cultured in 2COL, 1COL/2CS, 0.5COL/2CS, 2CS hydrogels for 1, 3, 5 days. The live cells are dyed green, and the dead cells are red. Scale bars, 100 μm. (b) Filamentous actin (F-actin) staining of RMCs after being cultured for 3 days. Scale bars, 20 μm. For interpretation of the references to color in this figure legend, the reader is referred to the web version of this article.

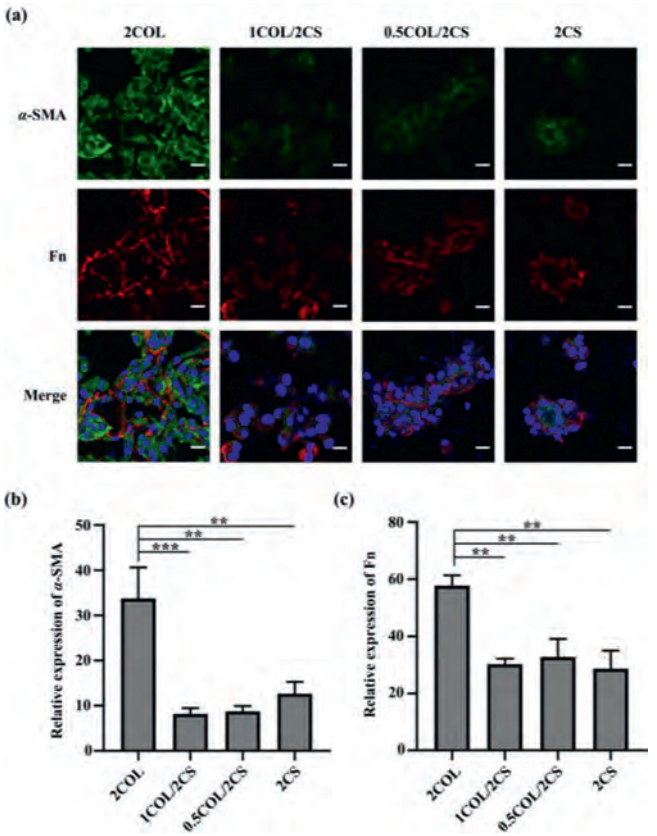

Fig. 4. (a) Immunofluorescence staining for expression of α-SMA (green) and fibronectin (Fn, red) proteins in RMCs seeded on biomimetic porous hydrogels after 3-day culture. Scale bars, 20 μm. Statistical analysis of mean fluorescence intensity for (b) α-SMA and (c) Fn proteins. All data are presented as mean ± SD. $^{**}P < 0.005$, $^{***}P < 0.0005$. For interpretation of the references to color in this figure legend, the reader is referred to the web version of this article.

Fn protein level was also detected using western blot analysis in the 2COL group compared with that in 2CS and COL/CS groups. Mesangial cells (MCs) play critical roles in the initiation and progression of glomerulosclerosis [41]. Under abnormal stimulus, MCs could transform into myofibroblasts and then secrete accumulated mesangial matrix (MM) such as COL I, Fn and α-SMA [42]. As consequences, abnormal COL I accumulation drive secretion of ECM and further cause the progression of fibrosis. Thus, pure COL I microenvironment could not facilitate kidney functional regeneration. With the addition of CS into the hydrogel, the expression of Fn and α-SMA in the located RMCs decreased. However, CS is endowed with an anti-fibrotic property, and our results showed that pure 2CS hydrogel also reduced the expressions of Fn and α-SMA proteins, but it has been reported that CS could inhibit cell migration and adhesion [43]. So pure CS microenvironment was adverse to *in vivo* endogenous cell recruitment, migration and adhesion to the scaffold. Considering the inherent advantages of COL I and CS in tissue engineering, we designed a biomimetic porous hydrogel scaffold using COL I incorporated with CS. CS had been reported to have anti-fibrotic properties [23,24] and its incorporation into scaffold could minimize the formation of native fibrosis *in vivo* to induce effectively renal tissue repair in damaged kidney *via in situ* tissue engineering.

To demonstrate the renal repair capability of implanted scaffolds *in vivo*, the different hydrogel scaffolds were transplanted into partially nephrectomized areas of the rat with left renal partially resected and right renal totally removed (partially nephrectomized rat). The renal repair effects of engrafted scaffolds were evaluated by examination of the renal function and analysis of histological staining. The renal function was evaluated through metabolic analysis (Fig. 5b). Compared with the injured rat without scaffold transplantation, the rat implanted with 1COL/2CS scaffold showed a significant amelioration of the renal dysfunction detected by valuation of metabolic markers such as serum creatinine (Scr) and blood urea nitrogen (BUN) concentrations. At week 4 after transplantation, the decreases of both BUN and Scr concentrations in 1COL/2CS rats had statistical significance compared with those in the other rats with kidney injuries, while no significant difference among the 2COL, 2CS and non-transplanted rats. The 1COL/2CS rat exhibited the largest function amelioration among all of rats with kidney injuries. With biofunctional support, the 1COL/2CS scaffold restored the kidney injury much faster because of the collaborative effect of COL and CS on host kidney cells, as contrasted with the other implanted scaffolds. At week 8 after operation, all rats with partial nephrectomy were examined to have a steady decrease of BUN levels, but the samples from the 1COL/2CS implanted group demonstrated a slightly lower level of BUN than those from the injured rats transplanted with 2COL or 2CS scaffolds or without graft. For creatinine concentration, despite having a lower level in 1COL/2CS group compared with injured group without graft, there was almost no difference among 2COL, 1COL/2CS and 2CS groups. These data imply that the effective improvement of metabolic function of kidney induced by 1COL/2CS scaffold is due to the interaction between cells and functional scaffold. The 1COL/2CS biomimetic matrix offered a functional platform to facilitate the renal recovery after injury.

Furthermore, the repair effects of the scaffold for damaged renal tissue were assessed through H&E and Masson staining and many host cells were observed in the scaffold-grafted areas (Fig. 6). After 8 weeks of transplantation, many host cells were recruited

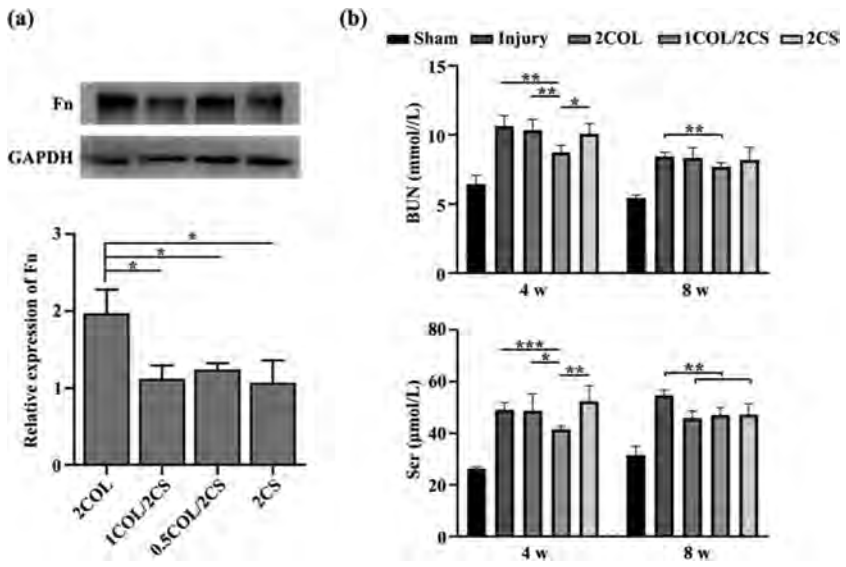

Fig. 5. (a) Western blot and Quantitative analysis of Fn protein expression of RMCs seeded on biomimetic porous hydrogels after being cultured *in vitro* for 3 days. (b) Renal function in all of the rats after operation was evaluated at 4 and 8 weeks by measurement of blood urea nitrogen (BUN) and serum creatinine concentration. All data are presented as mean ± SD. $^{*}P < 0.05$, $^{**}P < 0.005$, $^{***}P < 0.0005$.

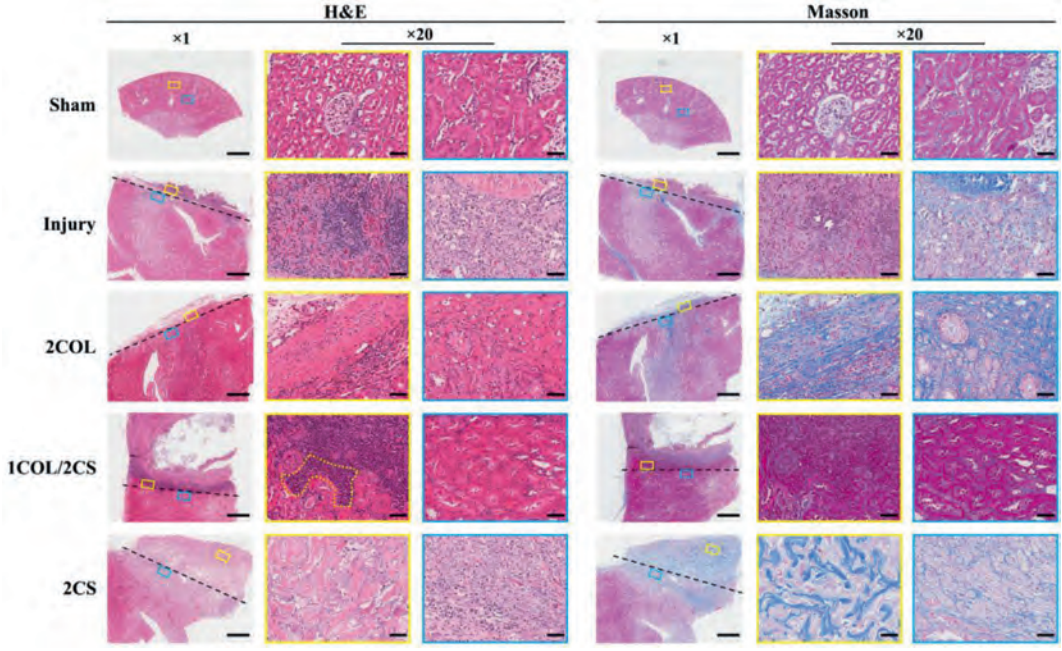

Fig. 6. *In vivo* evaluation of renal tissue regeneration capabilities in partially nephrectomized rats by H&E and Masson staining at 8 weeks. The dotted lines represent the sites of surgical resection. The areas of implanted scaffolds in 2COL, 1COL/2CS, 2CS group and inflammation infiltration in injury group located above the dotted lines which were represented with yellow rectangle while native renal tissues located below the dotted lines were represented with blue rectangle. × 1, scale bars, 1 mm; × 20, scale bars, 50 μm. For interpretation of the references to color in this figure legend, the reader is referred to the web version of this article.

into the renal resection areas with the degradation of scaffold. Interestingly, neonatal renal tubule-like structures were observed in the renal resection areas in the 1COL/2CS group (Fig. 6 and Fig. S3 in Supporting information). Additionally, the native renal tissues below the boundary between the kidney parenchyma and the scaffolds were virtually undamaged in 1COL/2CS group. In the damaged rats without implanted scaffold, quantities of inflammatory cell infiltrations were observed in the injured areas and seriously damaged renal tubules were detected near the renal resection areas accompanying with tubulointerstitial fibrosis. For rats transplanted with 2COL or 2CS scaffolds, some fibrotic connective tissue appeared near the renal resection areas with the degradation of the scaffolds and certain degrees of damage in renal tubules were detected below the renal resection areas. 2COL hy-

drogel was made up of pure COL I endowed the scaffold with easy degradation and the located cells are easily subject to fibrotic growth under this kind of microenvironment [44]. We also found that 2CS hydrogel consist of pure CS, was also not suitable for cell adhesion and proliferation [39,45]. However, the extracellular matrix-mimicking 1COL/2CS hydrogel with 3D porous network exhibited high biocompatibility, excellent cell adhesion as well as anti-fibrotic function. The synergistic effect between COL I and CS endow the 1COL/2CS hydrogel with an excellent microenvironment for endogenous cells recruitment, migration, proliferation and differentiation. Our results implied that the bionic 1COL/2CS hydrogel was beneficial for renal repair *in situ*.

In summary, we developed an extracellular matrix-mimicking hydrogel using polysaccharide CS and COL I extracted from grass carp swim bladder. We found that the 1COL/2CS hydrogel exhibited excellent biocompatibility *in vitro* and helped to guide cell behaviors *in vivo*. When the 1COL/2CS hydrogel was transplanted into renal resection areas of the nephrectomized rat, low inflammatory reaction and reduced fibrosis were reached in the native tissue and at the grafted areas. The 1COL/2CS hydrogel could also increase endogenous cells recruitment, migration and differentiation. Renal tubule-like structures formed in the renal resection areas where the 1COL/2CS scaffold was decomposed. Furthermore, the developed 1COL/2CS bionic hydrogel could be severed as an in suit tissue engineering platform for renal repair. In conclusion, this study highlighted a functional scaffold for kidney tissue repair. More extensive investigations of these biomimetic scaffolds on their potential therapeutic functions in chronic kidney diseases need to be further studied.

Declaration of competing interest

The authors declare that they have no commercial and personal relationships with other people or organizations that can inappropriately affect our work. There is no professional or other personal interest of any nature or kind in any product, service and/or company that could be construed as influencing the position presented, or the review of the manuscript entitled.

Acknowledgments

The authors thank the National Natural Science Foundation of China (Nos. 81870489, 32071363, 52003113, 81670669), Science and Technology Projects of Guangzhou City (No. 201804020035), Guangdong Basic and Applied Basic Research Foundation (Nos. 2020A1515110356, 2021A1515010745), and Key Research & Development Program of Guangzhou Regenerative Medicine and Health Guangdong Laboratory (No. 2018GZR110104002) for their financial support.

Supplementary materials

Supplementary material associated with this article can be found, in the online version, at doi:10.1016/j.cclet.2021.04.043.

References

[1] A.C. Webster, E.V. Nagler, R.L. Morton, P. Masson, Lancet 389 (2017) 1238–1252.
[2] V. Jha, G. Garcia-Garcia, K. Iseki, et al., Lancet 382 (2013) 260–272.
[3] K.H. Moon, I.K. Ko, J.J. Yoo, A. Atala, Adv. Healthc. Mater. 99 (2016) 112–119.
[4] P.Y. Dankers, J.M. Boomker, E.W. Meijer, E.R. Popa, M.J. van Luyn, J. Control. Release 152 (2011) 177–185.
[5] Y.L. Yu, Y.K. Shao, Y.Q. Ding, et al., Biomaterials 35 (2014) 6822–6828.
[6] J.M. Aamodt, D.W. Grainger, Biomaterials 86 (2016) 68–82.
[7] Y. Zhu, Q. Zhang, X. Shi, D. Han, Adv. Mater. 31 (2019) e1804950.
[8] N. Annabi, A. Tamayol, J.A. Uquillas, et al., Adv. Mater. 26 (2014) 85–123.
[9] G. Liu, Z. Bao, J. Wu, Chin. Chem. Lett. 31 (2020) 1817–1821.
[10] K. Yue, G. Trujillo-de Santiago, M.M. Alvarez, et al., Biomaterials 73 (2015) 254–271.
[11] D. Joladarashi, P.V. Salimath, N.D. Chilkunda, Glycobiology 21 (2011) 960–972.
[12] L. Kjellén, U. Lindahl, Annu. Rev. Biochem. 60 (1991) 443–475.
[13] A. Sorushanova, L.M. Delgado, Z. Wu, et al., Adv. Mater. 31 (2019) e1801651.
[14] M.C. Lane, M. Solursh, Dev. Biol. 143 (1991) 389–397.
[15] C.D. Nandini, K. Sugahara, Adv. Pharmacol. 53 (2006) 253–279.
[16] A.I. Van Den Bulcke, B. Bogdanov, N. De Rooze, et al., Biomacromolecules 1 (2000) 31–38.
[17] A. Jongjareonrak, S. Benjakul, W. Visessanguan, T. Nagai, M. Tanaka, Food Chem. 93 (2004) 475.
[18] X. Zhang, M. Ookawa, Y. Tan, et al., Food Chem. 160 (2014) 305–312.
[19] C.J. Chang, R. Minei, T. Sato, A. Taniguchi, Int. J. Mol. Sci. 20 (2019) 5349.
[20] J. Yang, M. Shen, H. Wen, et al., Carbohydr. Polym. 230 (2020) 115650.
[21] F. Legendre, C. Baugé, R. Roche, A.S. Saurel, J.P. Pujol, Osteoarthr. Cartil. 16 (2008) 105–114.
[22] N.M. Melo-Filho, C.L. Belmiro, R.G. Gonçalves, et al., Am. J. Physiol. Renal Physiol. 299 (2010) F1299–F1307.
[23] B. Corradetti, F. Taraballi, S. Minardi, et al., Stem Cells Transl. Med. 5 (2016) 670–682.
[24] E. Renard, C. Chadjichristos, M. Kypriotou, et al., J. Cell. Mol. Med. 12 (2008) 2836–2847.
[25] N.E. Ustyuzhanina, M.I. Bilan, E.G. Panina, N.P. Sanamyan, A.S. Dmitrenok, Mar. Drugs 16 (2018) 389.
[26] R.O. Sousa, A.L. Alves, J. Biomater. Sci. Polym. Ed. 31 (2020) 20–37.
[27] L. Wang, J. Jiang, W. Hua, et al., Adv. Funct. Mater. 26 (2016) 4293.
[28] N. Annabi, J.W. Nichol, X. Zhong, et al., Tissue Eng. B: Rev. 16 (2010) 371–383.
[29] S.M. Lien, L.Y. Ko, T.J. Huang, Acta Biomater. 5 (2009) 670–679.
[30] S. McLaughlin, B. McNeill, J. Podrebarac, K. Hosoyama, V. Sedlakova, Nat. Commun. 10 (2019) 4866.
[31] E. Lih, K.W. Park, S.Y. Chun, et al., ACS Appl. Mater. Interfaces 8 (2016) 21145–21154.
[32] X. Yang, Z. Li, H. Liu, et al., Int. J. Boil. Macromol. 143 (2020) 190–199.
[33] S. Mathews, R. Bhonde, P.K. Gupta, S. Totey, J. Biomed. Mater. Res. B: Appl. Biomater. 102 (2014) 1825–1834.
[34] J.W. Nichol, S.T. Koshy, H. Bae, et al., Biomaterials 31 (2010) 5536–5544.
[35] R.G. Wells, Hepatology 47 (2008) 1394–1400.
[36] Y. Ni, Z. Tang, W. Cao, et al., Int. J. Boil. Macromol. 74 (2015) 367–375.
[37] M. Hu, E.U. Azeloglu, A. Ron, et al., Sci. Rep. 7 (2017) 43934.
[38] A.J. Engler, S. Sen, H.L. Sweeney, D.E. Discher, Cell 126 (2006) 677–689.
[39] M. Yamagata, S. Suzuki, S.K. Akiyama, K.M. Yamada, K. Kimata, J. Biol. Chem. 264 (1989) 8012–8018.
[40] H.S. Tran, F.A. Chrzanowski, M.M. Puc, et al., J. Surg. Res. 88 (2000) 78–87.
[41] Y.M. Scindia, U.S. Deshmukh, H. Bagavant, Adv. Drug Deliv. Rev. 62 (2010) 1337–1343.
[42] R. Ortega-Velazquez, M. Gonzalez-Rubio, M.P. Ruiz-Torres, et al., Am. J. Physiol. Cell Physiol. 286 (2004) C1335–C1343.
[43] S. Bang, U.W. Jung, I. Noh, Tissue Eng. Regen. Med. 15 (2018) 25–35.
[44] C. Knupp, J.M. Squire, Adv. Protein Chem. 70 (2005) 375–403.
[45] R. Chiquet-Ehrismann, Curr. Opin. Cell Biol. 7 (1995) 715–719.